Advances in Applied Energy 4 (2021) 100071

Contents lists available at ScienceDirect

Advances in Applied Energy

journal homepage: www.elsevier.com/locate/adapen

The effect of non-spherical platinum nanoparticle sizes on the performance and durability of proton exchange membrane fuel cells

Xiaoyu Tan, Samaneh Shahgaldi, Xianguo Li*

Department of Mechanical and Mechatronics Engineering, University of Waterloo, Waterloo, ON, Canada N2L 3G1

ARTICLE INFO

Keywords:
Pt/C catalysts
Pt particle sizes
Mass activity
Durability
Proton exchange membrane fuel cells (PEMFC)

ABSTRACT

Platinum (Pt) nanoparticles with different sizes of 2 nm and 5 nm supported on functionalized high surface area carbon (HSC) have been successfully synthesized with a one-pot synthesis technique in large scale. Of the interest for the proton exchange membrane fuel cell applications, the synthesized supported catalysts are evaluated by physical characterizations, half-cell and scaled up single cell tests to study the impact of the catalyst sizes on cell performance and durability. Physical characterizations clearly demonstrate the sizes, shapes, crystallinity phases, and the total loading of the Pt nanoparticles on HSC. Half cell characterizations demonstrate higher electrochemical surface area, higher mass activity, and less durability for the working electrode prepared by the smaller Pt nanoparticle sizes (2 nm) than the larger Pt nanoparticles (5 nm). Scaled up single cell tests using air and hydrogen as the cathode and anode reactants demonstrate the membrane electrode assembly (MEA) prepared by smaller Pt nanoparticle sizes (2 nm) shows the maximum power density of 1.1 W/cm^2, which is 7% higher than the maximum power density of MEA prepared by larger Pt nanoparticles (5 nm) under similar operational conditions. The 30,000 cycles of accelerated stress test on the membrane electrode assembly prepared by larger Pt nanoparticles (5 nm) demonstrates 13% drop at maximum power density, illustrating the excellent performance against degradation (ageing).

Introduction

Hydrogen and fuel cells have become the essential and key elements of strategies for climate change mitigation and post-pandemic economic recovery, and have been incorporated into the core strategies for carbon neutrality by the middle of this century and greenhouse gas emission peaking by around 2030 for major economies around the world. Proton exchange membrane fuel cell (PEMFC) converts the chemical energy in hydrogen and oxygen directly into electrical energy through a key step of oxygen reduction reaction (ORR) [1]. Compared to the conventional energy conversion devices, it has many advantages, including low temperature operation, zero emission, and high efficiency [2]. These advantages make it promising for both stationary and mobile applications [3]. One of the key limitations to the commercialization of the PEMFC at this stage is its high cost [4]. Because of the low temperature operation, platinum (Pt) based catalyst is almost necessary for the ORR [5] in the practical PEMFCs in order to have sufficient performance and durability; however, Pt-based catalyst layer accounts for up to 41% of the overall cost of the fuel cell in mass production, which makes it difficult for the PEMFCs to be used on a large commercial scale [6].

A number of measures can be taken to lower the cost of Pt-based catalysts in PEMFCs, for example, lowering the cost of catalyst fabrication through improvement of the fabrication techniques, lowering the Pt loading through improvement of catalyst activities, and improving catalyst utilization in the PEMFC environment [7–9]. Since catalyzed reaction such as ORR occurs at the catalyst surface, traditional approach is to make the Pt particles smaller so that for a given amount of Pt mass (or volume), the electrochemical surface area (ECSA) of the Pt is substantially increased, hence the mass activity (MA, activity on a per unit mass of Pt basis) can be improved [10]. Nesselberger et al. [11] tested a series of different sizes of Pt nanoparticles ranged from 1 nm to 5 nm supported on the high surface area carbon (HSC) for ORR activities using half-cell tests and observed the trend of decreasing in ECSA and MA with the increase of the particle size. Smaller sized Pt nanoparticles can be obtained by controlling the synthesis conditions [12]. However, if the nanoparticle sizes are too small, it can counteract the advantages of the increased surface area because of the blockage of the reaction sites arising from the adsorption of competing molecular species [13]. Also, smaller nanoparticles are more prone to size growth during operations because of the high specific surface energy of nanoparticles [14,15]. In PEMFC environment, agglomerated Pt nanoparticles cause ECSA reduction, and therefore decrease the cell performance. Pt nanoparticles with the size ranged from 2 nm to 4 nm are reported to have the highest mass activity for ORR [16]. After comparing the performance of a series of Pt nanoparticles sizes from 1.6 nm to 2.6 nm, Wikander et al. [17] concluded that there is no apparent relation between the particle size and the ORR performance within the tested particle size range in half-cell

* Corresponding author.
E-mail address: Xianguo.Li@uwaterloo.ca (X. Li).

https://doi.org/10.1016/j.adapen.2021.100071
Received 16 March 2021; Received in revised form 30 September 2021; Accepted 30 September 2021
Available online 2 October 2021

tests; however, their impact in single cell performance and durability was not investigated.

The degradation of the catalyst layer appears through agglomeration/dissolution/detachment of Pt nanoparticles and carbon corrosion [18]. Holby et al. [19] analyzed the impact of Pt nanoparticle size on the stability of the catalyst via half-cell tests and simulations and concluded that increasing particle size will drastically improve the stability. Borup et al. [20] found that the growth rate of the size of the Pt nanoparticles is accelerated by high cycling potentials under high relative humidity (RH), which leads to lower ECSA. Xu et al. [21] tested stability of the Pt nanoparticles sized from 2.9 nm to 6.5 nm via in situ electrochemical test in a single-cell setup with an active area of $5cm^2$ for up to 1300 driven potential cycles between 0.6 V and 1.2 V, and the results demonstrate that larger Pt nanoparticles have reduced surface defects which improve the durability of the electrocatalysts. A recent study by Yano et al. [22] noted that the durability of Pt nanoparticles on carbon support is almost independent of the particle size if the particles are evenly dispersed and the size is uniform (with standard deviation smaller than 10%). They compared carbon supported Pt nanoparticles of size 2 nm and 4 nm before and after 30,000 cycles between 0.6 V and 1.0 V vs. reversible hydrogen electrode (RHE) using half-cell tests. Despite the research effort on the performance of the Pt nanoparticles of different sizes, there are many discrepancies in literature and few studies focused on the impact of Pt nanoparticles sizes on durability of the catalyst layer via scaled up single cell. As a result, a comprehensive analysis including both half-cell and full-cell characterization would be important to fully understand the impact of the size of the Pt nanoparticles on PEMFC's overall performance and durability.

For the factors influencing the durability and performance of the fuel cell, in addition to the sizes, the dispersion of the Pt nanoparticles also has a huge impact [23]. One of the most important parameters determining the catalyst dispersion is selecting the proper support material. High surface area substrate is required to support small-sized Pt particles to counter the particle-size effect [24,25]. Various allotropic varieties of carbon have been widely and commercially used as the support material for precious metal catalysts due to its high surface area, porous nature, electrical conductivity and many other advantages [26]. Among these, HSC shows promising results as a catalyst support due to the listed advantages and has the benefit of high availability and low cost [24]. The surface of HSC is usually chemically modified to interact favorably with the Pt nanoparticles and leads to better catalyst dispersion [27,28].

The synthesis process of the catalyst also has significant impacts, because it is the synthesis process that controls the Pt nanoparticle size and the dispersion of Pt nanoparticles on the supports [29–31]. The state-of-the-art of Pt catalyst on carbon support is synthesized via different methods like impregnation-reduction, microemulsion, ion exchange, sputtering, polyol and many others [32]. Among these methods, a simple and reproducible loading method that has control over the Pt nanoparticle size and dispersion would be ideal for mass production. In general, it is conventional that Pt nanoparticles are synthesized first, and then deposited on the carbon-based substrate through various techniques during the fabrication of the Pt-based catalysts [33,34]; this two-step process increases the complexities of catalyst fabrication and limits the rate, and hence increases the cost, of catalyst production [35]. It would be preferred if the Pt-based catalysts can be produced in a simple one-step process with large quantities (scaled up) to reduce the cost of the catalyst production.

Further, it is conventional that most of the catalyst development is based on the half-cell characterizations, and it is also known that catalysts with good characteristics exhibited in half-cell tests are often not necessarily good in full cell tests. This is because half-cell characterizations of the catalysts use liquid electrolyte and provide the electrochemical properties of the catalyst materials, while the full fuel cell uses solid polymeric membrane as the electrolyte, and the full cell test results reflect the overall balance between the electrochemical kinetics and transport phenomena occurring in the catalyst layers of the cell. Whereas the catalyst layers consist of not only supported catalyst particles on which catalyzed electrochemical reactions occur and through which electron transports, but also ionomer thin film covering the catalyst surface to form the three-phase boundary and through which proton transports, and porous region among the catalyst agglomerate structures for reactant transport and product removal. Furthermore, conventional catalyst material research involves the synthesis of the catalyst material in a very small amount using various nano-techniques, and stops their work after the half-cell characterization of the synthesized catalyst nanoparticles; whereas practicing engineers would work with large full cells of practical application. Very few studies in literature have, in a single study, taken the complete process from the synthesis of catalyst materials in large quantities, conducted half-cell characterizations to verify the good catalytic properties of the synthesized catalyst materials, then fabricated full fuel cells of large size with proper techniques, and finally tested to demonstrate the performance and durability of the fuel cells developed.

The objective of the present study is therefore to develop high surface area Pt nanoparticles with different sizes on HSC via a simple and one-pot synthesis method, and to demonstrate the viability of the produced catalyst for large sized fuel cells for practical applications. In this study, a simple one-pot process is first developed to synthesize the intended Pt-based supported catalyst in large quantities (i.e., scaled up production of the catalyst materials), then comprehensive physical and electrochemical ex-situ and in-situ characterizations are conducted to elucidate the impact of Pt nanoparticles sizes on the performance and durability of the developed catalysts through both half- and full- cell tests. The results obtained are used to explain the discrepancies in literature, and contribute to the development of the practical catalysts for commercial fuel cells.

2. Experiments

Material: HSC, hexachloroplatinic acid (H_2PtCl_6), hydrochloric acid (HCl), nitric acid (HNO_3), sulfuric acid (H_2SO_4), sodium hydroxide (NaOH), Ethylene Glycol (EG), de-ionized water (DI), perchloric acid ($HClO_4$).

2.1. Carbon support and surface functionalization

In a typical carbon support functionalization setup, HSC is mixed with HCl and refluxed at 120 ˚C. The sample is then separated using centrifugal separator to collect the HSC and washed with de-ionized water (DI) and collected again. The collected sample is washed with DI water several times until reaching neutral pH. Next, the collected sample is mixed with the proper ratio of H_2SO_4 and HNO_3, heated at 120 ˚C for further functionalization. The functionalized HSC is collected after the sample is washed to neutral pH with DI water using the same centrifugal separation methods.

2.2. Synthesis of Pt nanoparticles onto functionalized HSC

The synthesis is achieved using one-pot method, where the Pt nanoparticles deposit directly onto the functionalized HSC. First, 0.4 g of HSC is mixed with the solvent and reducing agent. Afterward Pt precursor added to the solution under nitrogen, while the solution is being mixed using the magnetic stirrer bar. The pH of the solution is set at 10 using NaOH, and the temperature is increased to 160 ˚C or 180 ˚C for controlling the size of Pt nanoparticles. The solution is held at the required temperature for 3 h and the pH is decreased to 2 using HCl. Synthesized Pt/C is then collected using centrifugal separator and washed with DI water several times until its pH reaches 6. The final product is dried under Ar atmosphere at 70 ˚C for 24 h.

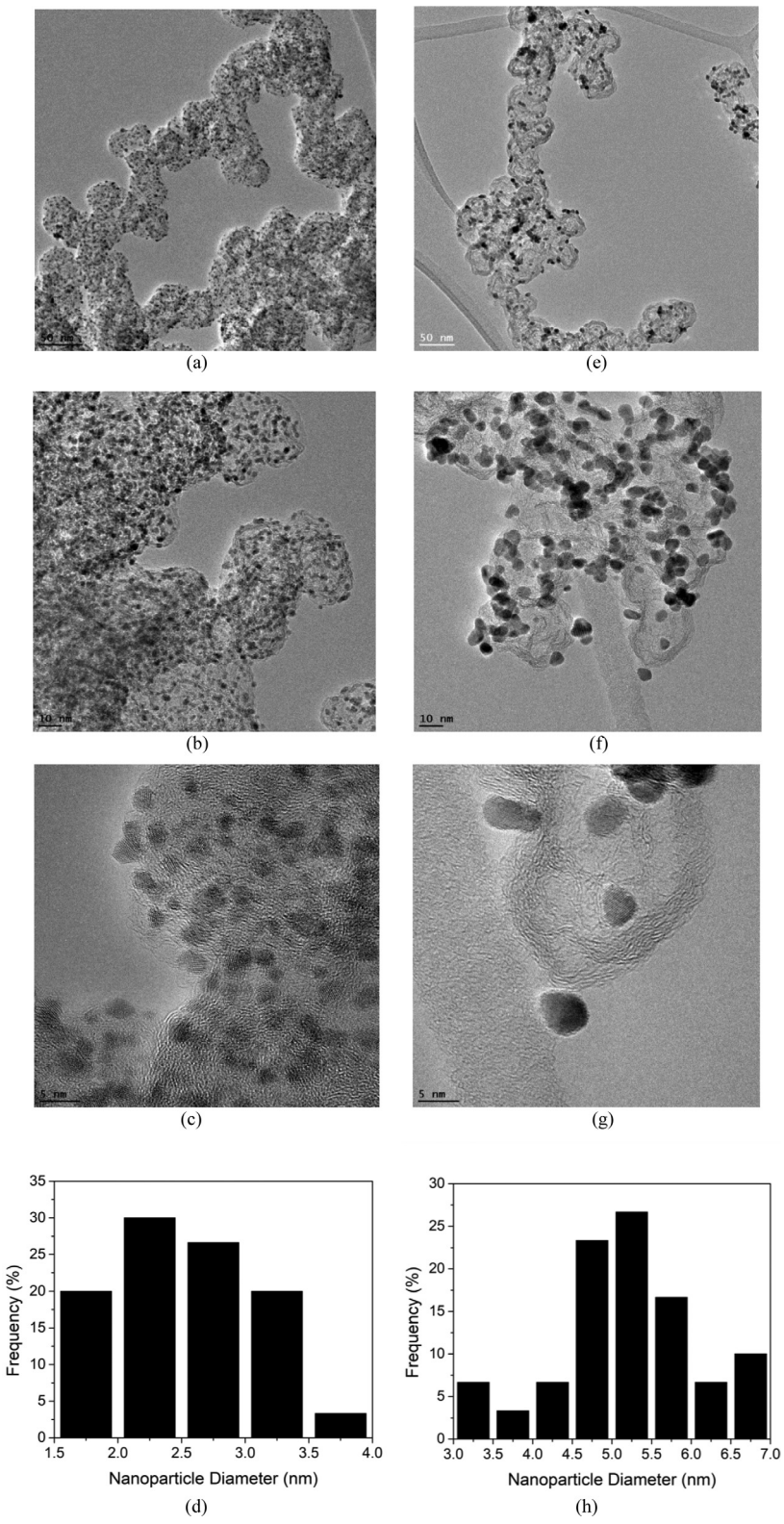

Fig. 1. TEM images of the synthesized HSC-Pt at the reaction temperatures of 180 °C (a-c) and 160 °C (e-g) at the different magnifications, and the Pt nanoparticle size histograms related to the reaction temperature of (d) 180 °C, and (h) 160 °C.

2.3. Physical characterizations

The thermogravimetric analysis (TGA) is used to determine the Pt loading (weight percentage of Pt) of the samples. By increasing the samples to 800 °C under air flow, most of the carbon is burnt off. To calculate the exact weight of Pt, the carbon is tested in TGA separately as the baseline to obtain the weight residual of carbon; by eliminating the weight residual of the carbon, the remaining weight to the total weight of the sample is the Pt loading. X-ray diffractograms (XRD) of the samples are recorded for the 2θ angle region to determine the crystallite planes of the Pt nanoparticles. The sample images are captured using transmission electron microscopy (TEM) operating at 300 kV with magnification between 2250x to 360kx for the dispersion and size of the Pt nanoparticles synthesized.

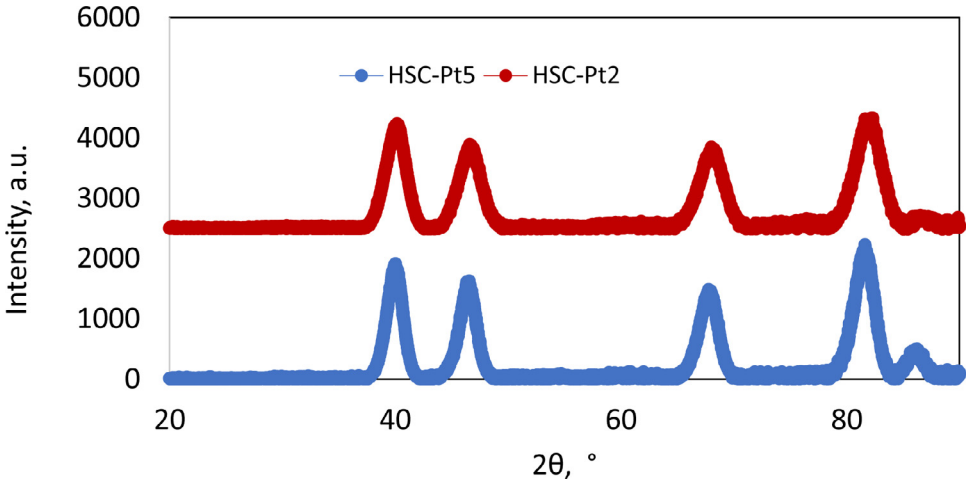

Fig. 2. XRD patterns of the synthesized HSC-Pt at two different reaction temperatures: 180 °C (HSC-Pt2) and 160 °C (HSC-Pt5).

2.4. Ex-situ electrochemical characterizations

All the half-cell electrochemical measurements are carried out using CH-Instruments 760E Bi-potentiostat coupled with BAS RRDE-3A rotating disk electrode system. Glassy carbon (GC) disk with 4 mm diameter is used as working electrode, RHE and Platinum wire are used as reference electrode and counter electrode, respectively. 0.1 M $HClO_4$ saturated with N_2/O_2 is used as electrolyte. Catalyst ink is prepared using 5 mg of catalyst in 5 ml of de-ionized (DI) water, ethanol mixture in the ratio 1:9 by percentage and 30 μL of ionomer. The suspension is sonicated until homogenous dispersion of ink is formed. The working electrode is prepared by polishing glassy carbon disk with alumina slurry on a fiber pad, followed by thorough rinsing with DI water and air drying. A total of 6.4 μL aliquot of ink (containing 6.4 μg of catalyst) is drop casted onto the GC disk to make a uniform catalyst layer. The electrolyte is purged constantly with nitrogen gas for an hour to remove air from it prior to the cyclic voltammetry measurements and similarly purged with oxygen gas prior to linear sweep measurements. Durability studies for half-cell, or half-cell accelerated stress tests (AST), is carried out by cycling the potential of the working electrode between 0.5 V to 1 V Vs. RHE at the scan rate of 0.5 V/s for 3000 cycles.

2.5. In-situ electrochemical characterizations

A homogeneous ink is made by mixing the synthesized Pt/C catalyst with an ionomer, DI-water and iso-propanol. Afterwards the ink is sonicated for 1 h, then sprayed onto both surfaces of a membrane until the proper loadings are obtained. The catalyst loading in the anode and cathode sides are set at 0.1 and 0.4 mg/cm^2, respectively, while the Pt/C to ionomer ratios are set at 3/1 for both sides. The membrane coated with catalyst layers is sandwiched between the gas diffusion electrodes and sealed with Kapton gaskets. The active surface area of the fabricated membrane electrode assembly (MEA) is 45 cm^2. The prepared MEA is placed between two straight flow-field plates and compressed to ensure proper sealing with no leakage from either side. To assess the cell performance, two flow conditions of the reactants are applied: Low flow for the flow of hydrogen and air with stoichiometries of 1.2 to 2, and high flow for a constant flow rate of hydrogen and air at 4.45 and 9 slpm respectively. The cell backpressure and temperature are set at 35 kPag and 75 °C, respectively, for both flow conditions. In addition, the behavior of catalysts is evaluated under high (100%) and low (40%) relative humidities (RH). AST is carried out by cycling the cell voltages between 0.60 and 1 V for 30,000 consecutive cycles, at a scanning rate of 0.05 V/s. After finishing the AST, the polarization curves are plotted under high (100%), and low (40%) RHs at the constant temperature of 75 °C and 35 kPag. Electrochemical impedance spectroscopy (EIS) is measured before and after the AST at the cell voltage of 0.70 V, direct current with the amplitude of 10 mA, and frequency range of 100 mHz and 100 kHz.

3. Results and discussion

In this study, two sizes of Pt nanoparticles supported on HSC are obtained via controlling the one-pot synthesis reaction temperature. Fig. 1 (a-c, e-h) shows the TEM images and size distribution of the as-prepared Pt nanoparticles on HSC with two different sizes. As is clear from Fig. 1(a and e) Pt nanoparticles are uniformly dispersed on the HSC support without any noticeable agglomeration and increasing the reaction temperature results in smaller Pt nanoparticles. Fig. 1(b and f) demonstrate higher magnification of TEM images for both samples, which clearly show the size differences between the prepared catalysts. In the fast nucleation growth when the reaction temperature is high at 180 °C, the average particle size is around 2 nm (Fig. 1(c)); hence it is referred to as the catalyst HSC-Pt2 hereafter. At a lower reaction temperature of 160 °C, the average particle size is about 5 nm, which is referred hereafter as HSC-Pt5 (Fig. 1(g)). It is clear from the high magnification TEM images (Fig. 1(c and g)) that the shape of Pt nanoparticles is also impacted by reaction temperature; for instance, at the higher temperature of 180 °C all the nanoparticles are faceted, and at the lower reaction temperature of 160 °C they are almond and flat shapes. Higher magnification images are taken of the nanoparticles located on the carbon edges to gain better and clearer images about the shape of nanoparticles and the impact of carbon on Pt nanoparticle shapes. To obtain the size distributions of the prepared Pt nanoparticles on HSC, two size distribution histograms are plotted which are shown in Fig. 1 (d and h) related to the HSC-Pt2 and HSC-Pt5, respectively. As Pt nanoparticles are not spherical, the diameter is measured by taking the average of the lengths across and along the elongated direction. Based on histograms the average particle size is estimated to be around 2.49 nm for HSC-Pt2 and 5.19 nm for HSC-Pt5.

Fig. 2 presents the XRD pattern of the synthesized HSC-Pt2 and HSC-Pt5 catalysts, illustrating the characteristics of the property of the crystalline Pt face's centered cubic (fcc) phase. The peaks are located at 40°, 46.5°, 67.9°, 81.6°, and 86.3°, and are assigned to 111, 200, 220, 311, and 222 crystallographic planes, respectively. XRD peaks of the synthesized HSC-Pt2 and HSC-Pt5 are comparable with those corresponding to bulk Pt and commercial Pt/C catalysts reported in literature [36]. Based on the Debye-Scherrer equation, the particle sizes of HSC-Pt2 and HSC-Pt5 are estimated as, respectively, 3 nm and 5 nm, which are consistent with the observations from the TEM images shown earlier. Therefore, the particle sizes estimated from the TEM images are considered as more reliable, while XRD results provide a good confirma-

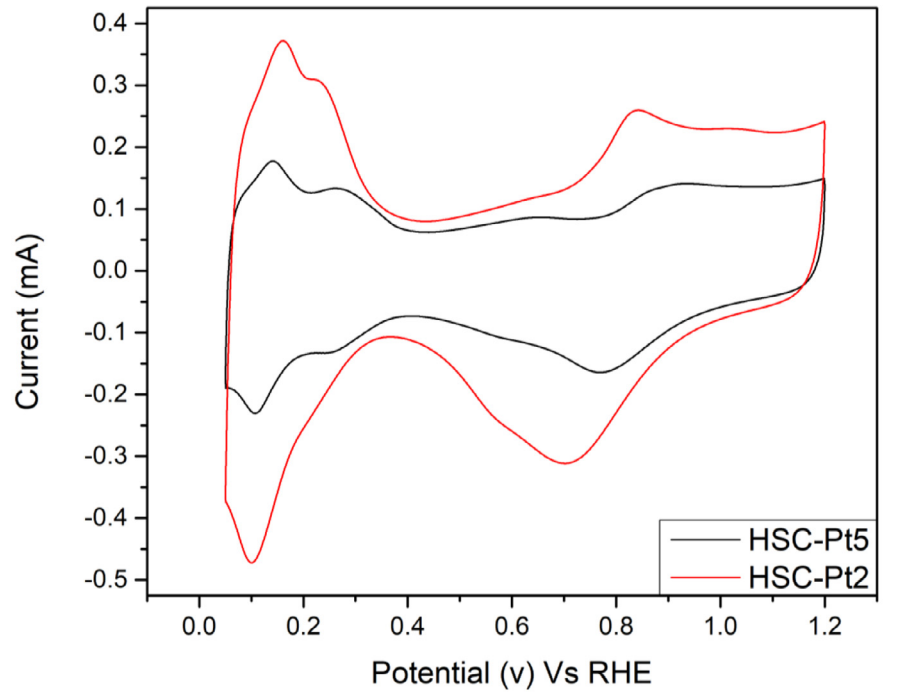

(a)

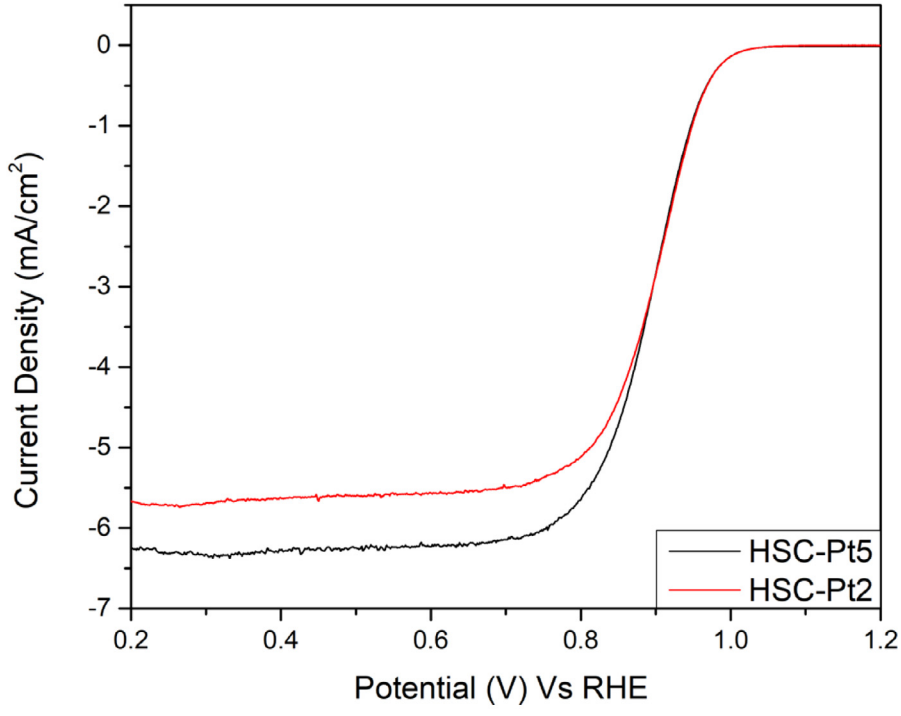

(b)

Fig. 3. Half-cell electrochemical characteristics comparison between the HSC-Pt2 and HSC-Pt5: (a) cyclic voltammograms; and (b) linear sweep voltammetry at the rotation speed of 1600 rpm.

tion of the Pt particle sizes estimated from the TEM images. In order to obtain the accurate Pt loading on the support, the thermogravimetric analysis (TGA) is conducted on both samples. Based on the TGA results, HSC-Pt2 and HSC-Pt5 have approximately 45.4% and 47.6% Pt loading, respectively.

Half-cell tests are conducted to compare the electrochemical characteristics of the HSC-Pt5 and HSC-Pt2 samples. The change of the hydrogen adsorption and desorption areas for the prepared catalysts is shown in Fig. 3(a). The electrochemical surface area is calculated from the hydrogen desorption charge integrated under relevant potential range according to the hydrogen standard electrode when, on the Pt surface, adequate charge to oxidize a monolayer of hydrogen is considered as 210 $\mu C/cm^2$ [37,38]. As it is clear from the figure, HSC-Pt2 shows higher hydrogen desorption peak, and has higher ECSA of 82.10 m^2/g, while

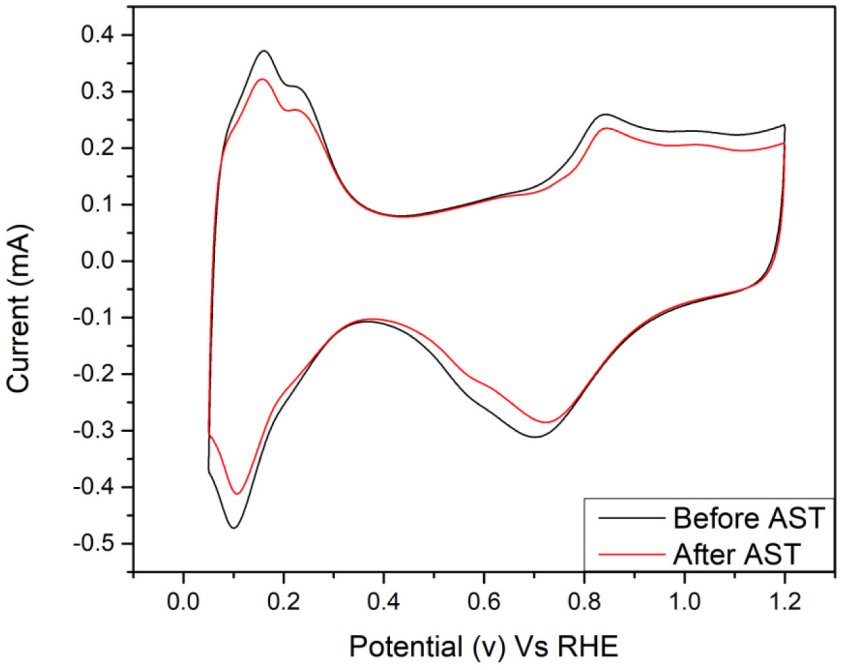

(a)

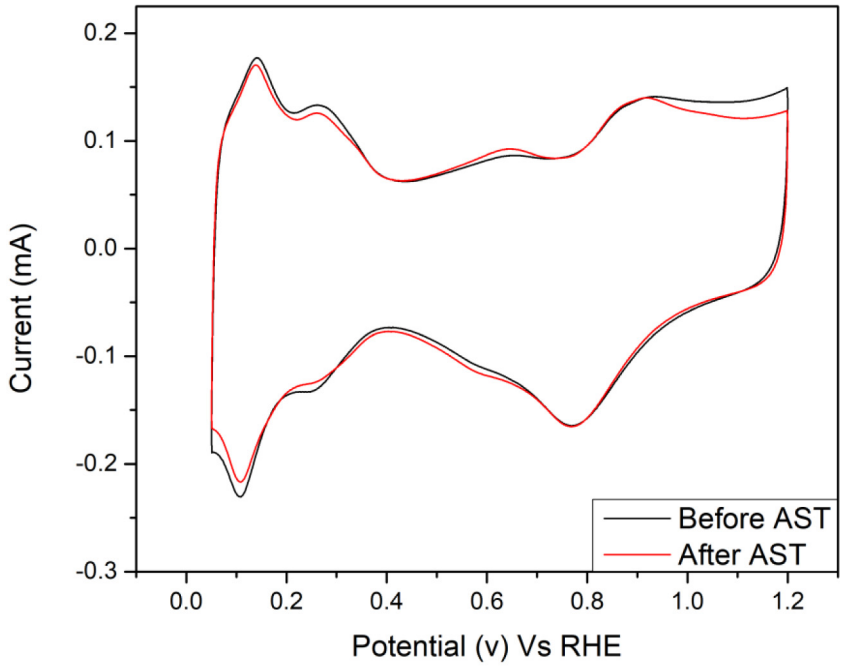

(b)

Fig. 4. Half-cell electrochemical characteristics: cyclic voltammograms taken before and after the ASTs (a) HSC-Pt2 and (b) HSC-Pt5.

HSC-Pt5 has ECSA of 31.08 m^2/g. Therefore, with similar Pt loading, the HSC-Pt2 sample achieves 2.64 times of ECSA compared to HSC-Pt5 by reducing the size of the Pt nanoparticles. In order to elucidate the influence of these two Pt nanoparticle sizes on the catalyst activity for ORR, both prepared catalysts are studied by running the linear sweep voltammetry (LSV) curves on rotating disk electrode at 1600 rpm under the oxygen saturated environment. As can be seen in Fig. 3(b), the current densities at onset potentials of ORR at 0.9 V for HSC-Pt2 and HSC-Pt5 are 2.85 and 2.84 mA/cm^2, respectively, and the diffusion limiting current densities are 5.69 and 6.33 mA/cm^2, respectively, at 0.3 V (Vs RHE). The higher diffusion-limiting current density at 0.3 V for HSC-Pt5 indicates that the larger sized Pt catalyst has less of its particles falling into the surface pores of the support HSC [39], hence relatively less resistance to reactant diffusion to the active catalytic sites [40]. However, the lower value for HSC-Pt2 is indicative of the trapping of the small Pt nanoparticles in the porous structure of the HSC support

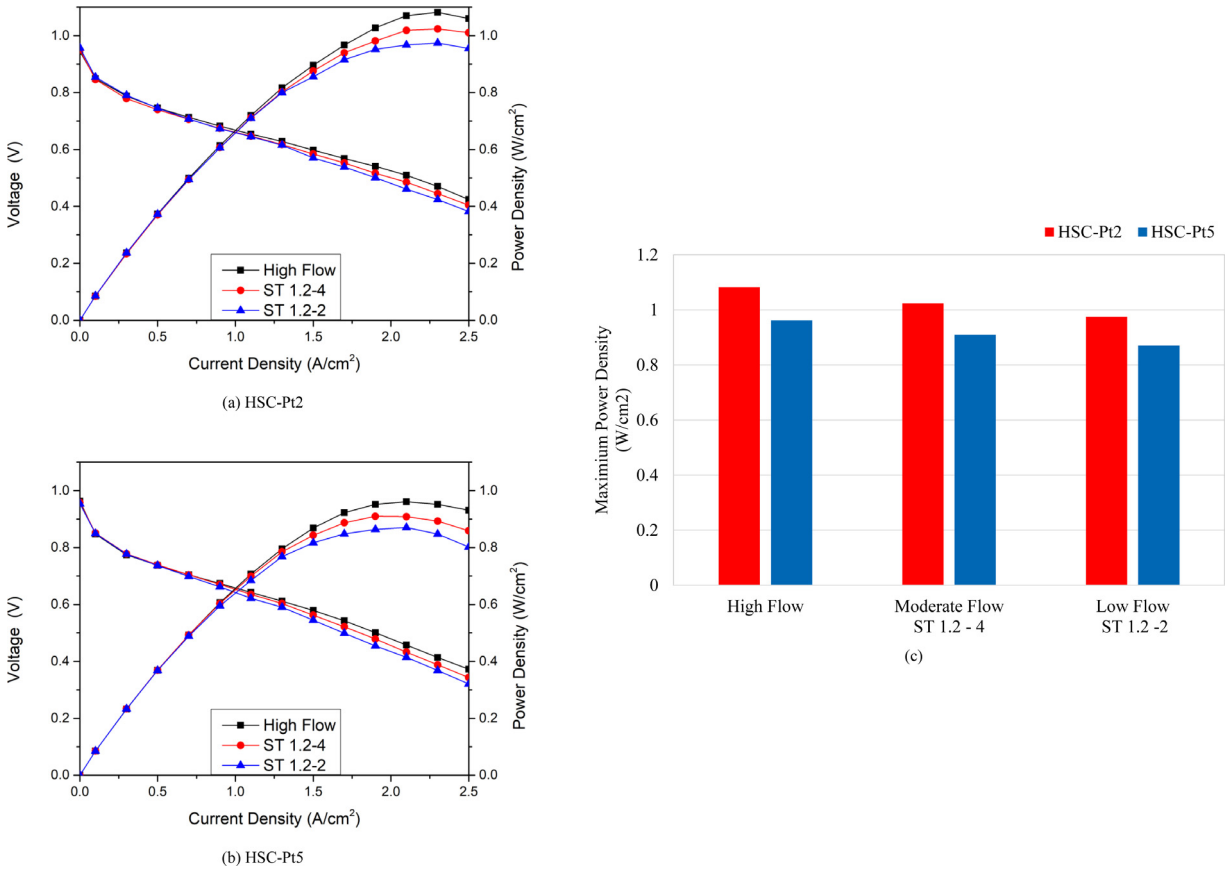

Fig. 5. Polarization and power density curves obtained from the MEAs with the catalyst of (a) HSC-Pt2 and (b) HSC-Pt5 under different flow conditions of the reactants, and (c) shows the comparison of the corresponding maximum power density.

[41], which hinders their accessibility to the reactants [42]. MA and surface specific activities (SA) are calculated, at 0.9 V by convention, to be 247.66 mA/mg and 301.65 μA/cm^2 for HSC-Pt2, and 212.45 mA/mg and 683.56 μA/cm^2 for HSC-Pt5, respectively. The non-spherical shape of the Pt nanoparticles of HSC-Pt5 contributes to the exposure of different planes of Pt, which increases its interaction of Pt nanoparticles with support and leads to higher SA, the similar trend is also observed in other studies as well [43].

The stability of the prepared catalysts is examined using the AST. Fig. 4 shows the cyclic voltammogram curves for the HSC-Pt2 and HSC-Pt5 before and after the 3000 cycles of AST from 0.5 V to 1 V at a scan rate of 0.5 V/s. It is shown that the hydrogen adsorption and desorption peaks' areas are reduced in both samples, and ECSA losses after 3000 cycles are about 14.6% for HSC-Pt2 and 6.0% for HSC-Pt5. As it is seen, HSC-Pt2 has less stability than HSC-Pt5 in acidic fuel cell environment after 3000 cycles. This can be explained by the higher surface area to volume ratio of the smaller nanoparticles, which tends to grow in size to decrease their surface free energy more easily.

To evaluate the impact of the synthesized catalysts on the PEMFC performance, and correlate ex-situ and in-situ electrochemical characterizations, scaled up MEAs with the active area of 45 cm^2 are prepared using the above two catalysts respectively through catalyst coated membrane method. The MEAs are tested under different operating conditions to elucidate the performances of the two catalysts. Fig. 5(a) and (b) show the polarization and power density curves of the prepared MEAs under fully humidified air and hydrogen streams. Three different flow rates – low, moderate, and high – of hydrogen and air are applied in the experiment. Hydrogen flow rates of 4.45 and air flow rates of 9 L/min are referred to as high flow, and hydrogen/air with the stoichiometric ratios of 1.2 /4 and 1.2/2 are given the name of ST 1.2–4 (moderate flow) and ST 1.2–2 (low flow), respectively. It is clear from Fig. 5(a) and (b) that both MEAs show a similar trend of variations under the different flows of reactants, and that the cell performances are improved by an increase in the reactant flows. The open circuit voltages (OCVs) are around 0.95 V under all three conditions for both MEAs. In the activation polarization regime, polarization curves are seen to be very close to each other under the different flows. For example, the cell voltage is approximately 0.85 V for both MEAs when the constant current density is at 0.1 A/cm^2. The same trend is also valid for the ohmic polarization region. For instant, the cell voltage is 0.7 V for both MEAs under all three conditions when the constant current density is at 0.7 A/cm^2. However, in the concentration polarization regime, at 2.1 A/cm^2 for example, the cell voltages drop by 8% from the high flow to the low flow conditions for both MEAs. Fig. 5(c) compares the maximum power densities of both MEAs under the different flows of reactants. It can be seen that MEA made by HSC-Pt2 has a higher maximum power density than the MEA made of HSC-Pt5 under all three flows of reactants. For example, the MEA made of HSC-Pt2 shows 8% and 13% higher maximum power densities in comparison to the MEA made of HSC-5 under the high and low flow (ST 1.2–2), respectively. The higher performance of MEA made of HSC-Pt2 can be explained via the smaller size of Pt nanoparticles with a higher ratio of surface atoms leading to higher Pt surface area and utilization and may improve the accessibility of Pt nanoparticles for the constant ionomer amount.

Fig. 6(a) and (b) illustrate the polarization and power density curves of the MEAs prepared with the HSC-Pt2 and HSC-Pt5 catalysts under three different flows of reactants when the RH is set at 40%. As clearly seen from the figures, both MEAs present completely different trends of variation from the results obtained under fully humidified (100% RH) condition, as the cell performance is improved by decreasing the flow of

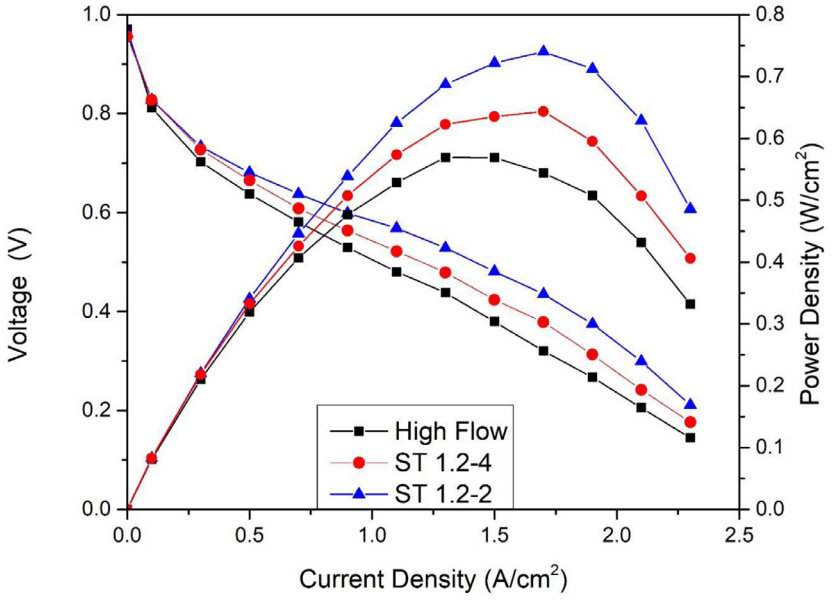

(a) HSC-Pt2

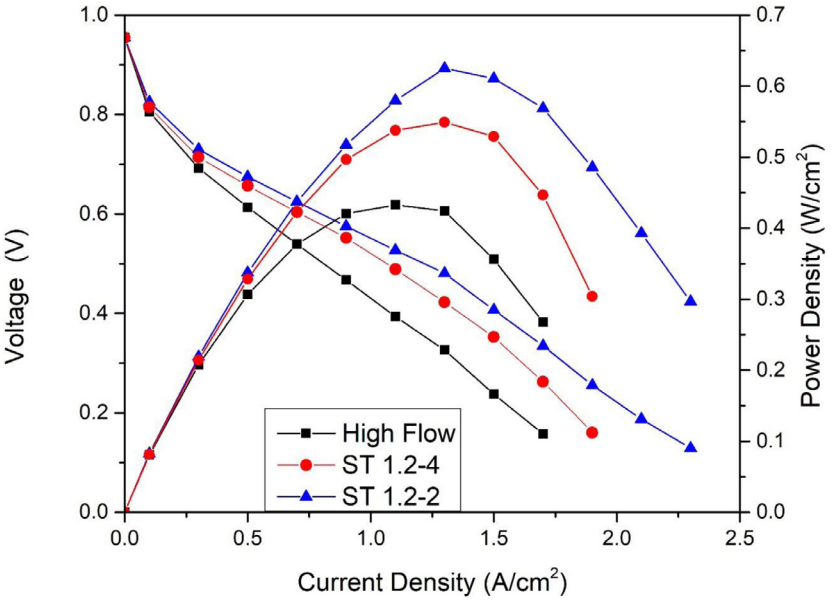

(b) HSC-Pt5

Fig. 6. Polarization and power density curves by the MEAs made with (a) HSC-Pt2, (b) HSC-Pt5 under different flow conditions of the reactants, with RH of 40% at anode and cathode.

reactants. This trend of variation is significant, because higher flow rates are normally expected to provide higher accessibility of reactants, and hence increased cell performance. However, it can be seen that a high flow of reactants actually results into a poorer performance under the present low RH operation, because of dehydration in the ionic phases of the MEAs. In the activation polarization regime, both MEAs show almost the same performance, and the difference starts in the ohmic and increases in the concentration polarization regimes. As shown in the figures, the cell voltages are at about 0.81 V for both MEAs under the high flow of the reactants when the constant current density is at 0.1 A/cm^2. However, the difference becomes appreciable beyond 0.5 A/cm^2. The cell voltages are around 0.63 V and 0.61 V with the high flow of the reactants when the current density is at 0.5 A/cm^2 for MEAs made of HSC-Pt2 and HSC-Pt5, respectively. These values rise to 0.66 V and 0.65 V with the moderate flow, and 0.68 V and 0.67 V with the low flow of the reactants. The maximum power density for the MEAs made of HSC-Pt2 and HSC-Pt5, under the low flow condition, is 0.74 W/cm^2 and 0.62 W/cm^2 respectively. In addition, it can be noted that under 100% RH (See Fig. 5) and 40% RH (See Fig. 6), the MEA made of HSC-Pt2 shows higher performance in comparison to the MEA made of HSC-Pt5.

In-situ electrochemical characteristics of the MEAs prepared with HSC-Pt2 and HSC-Pt5 are presented in Fig. 7. The curve shapes and hydrogen adsorption and desorption peaks are similar to those obtained in literature for MEAs prepared with commercial Pt/C catalysts [44]. It is clear that the MEA prepared with HSC-Pt2 has a higher hydrogen adsorption and desorption peaks than that with HSC-Pt5. The ECSAs are calculated based on the Pt loading, the hydrogen adsorption and desorption charges and the electrical charge associated with the monolayer adsorption of hydrogen on a Pt surface. The ECSA of the MEAs made with HSC-Pt2 and HSC-Pt5 are 73 m^2/g and 50 m^2/g, respectively.

Based on the ex-situ half-cell electrochemical characterizations, it is surmised that HSC-Pt2 has 164.2% higher ECSA and 16.6% higher MA

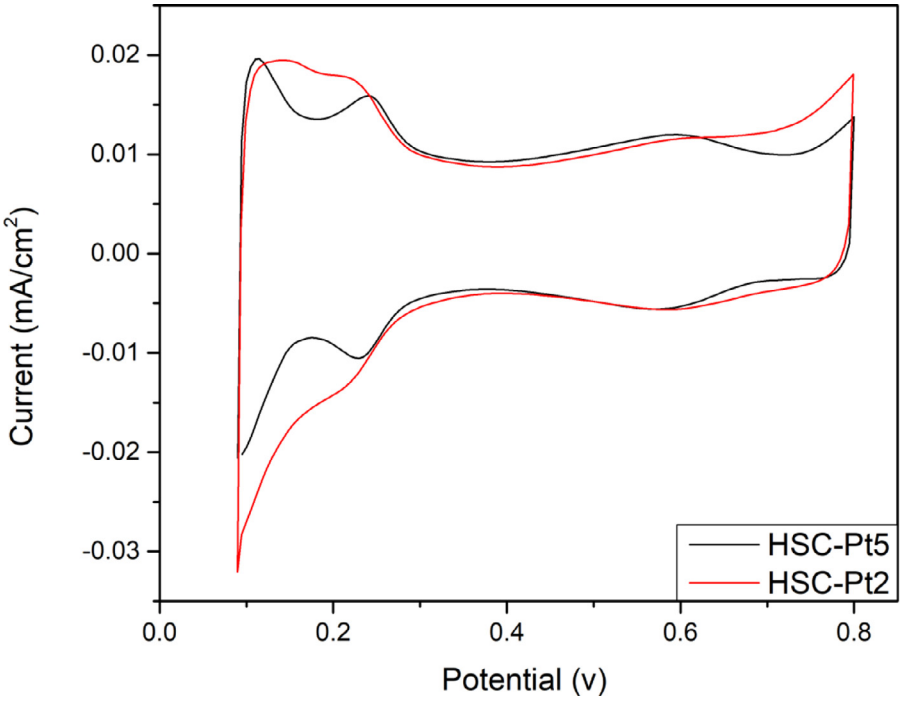

Fig. 7. Cyclic voltammograms for the MEAs prepared with HSC-Pt2 and HSC-Pt5 at 75 °C with back pressure of 35 kPag and RH of 100%.

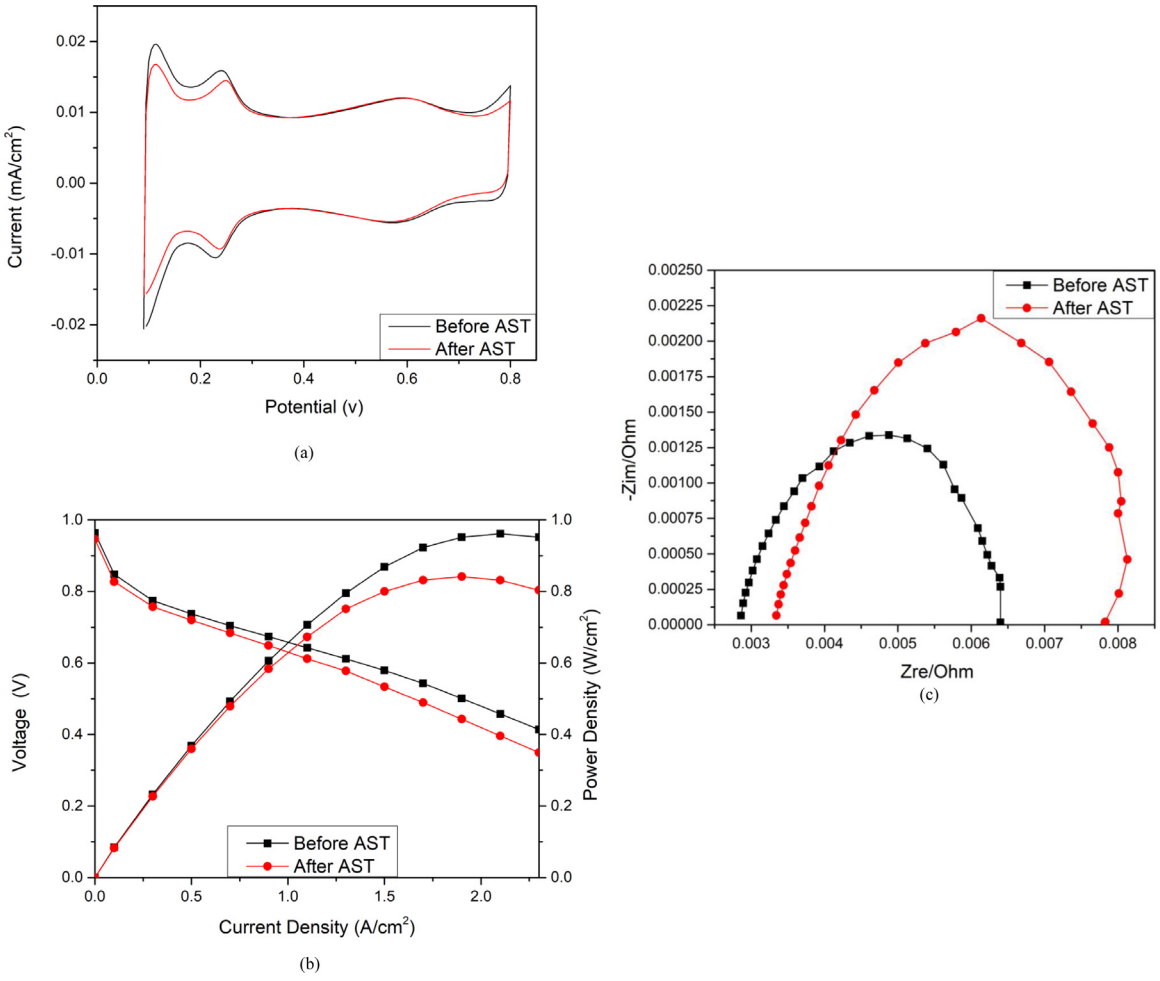

Fig. 8. Electrochemical characteristics of the MEA made of HSC-Pt5, before (0 cycle) and after the AST (30,000 cycles): (a) cyclic voltammograms; (b) Polarization and power density curves; (c) Impedance.

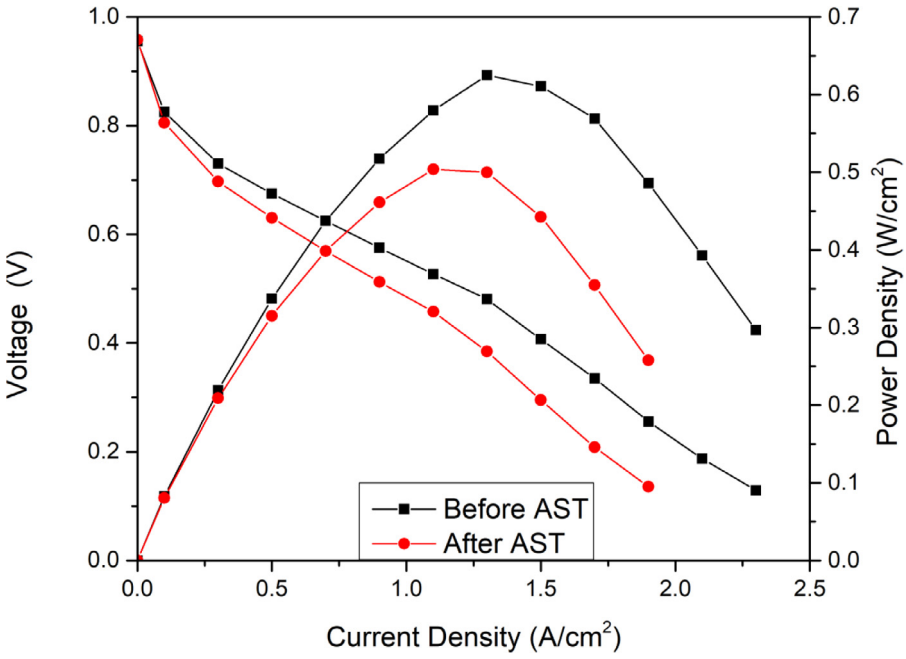

Fig. 9. Polarization curves and power density curves of the MEA made of HSC-Pt5 at 40% RH and low flow ST 1.2–2 before and after AST.

over HSC-Pt5, while the SA and durability are higher for HSC-Pt5 by 116.6% and 8.6%, respectively. In addition, the scaled up single cell performance indicates 10% higher maximum power densities for MEA made of HSC-Pt2 over HSC-Pt5 under the fully humidified condition. Despite lower fuel cell performance in the MEA made of HSC-Pt5 than that of HSC-Pt2, with the maximum power densities of 0.87 W/cm^2 as compared with 0.97 W/cm^2 under the fully humidified and low flow condition, it still demonstrates very promising results when it is compared with the performance made of other synthesized and commercial catalysts reported in literature [21,45–47]. As both the present catalysts demonstrate promising performance under different operating conditions, and half-cell data shows higher stability for HSC-Pt5, this catalyst is selected for further investigations.

In order to evaluate the loss of active surface area for MEAs made of HSC-Pt5, in-situ cyclic voltammetry is carried out, at a cell temperature of 75 °C, backpressure of 35 kPag and RH of 100%. Fig. 8(a) shows the cyclic voltammograms before and after the AST. It is clear that the hydrogen adsorption and desorption peaks are reduced after 30,000 cycles. The ECSA values are reduced by 18% after 30,000 cycles. This reduction in the electrochemical characteristics could represent 3% reduction of the open circuit voltage (OCV) values as shown in Fig. 8(b). Fig. 8(b) shows the cell performance of the MEA prepared using HSC-Pt5 before and after the AST under the identical operating condition: cell temperature of 75 °C, back pressure of 35 kPag, 100% RH, and reactant flow rates of 4.45 slpm for the anode and 9 slpm for the cathode. As illustrated in the polarization curves, the OCV value slightly drops after 30,000 cycles, and the main reduction occurs in the ohmic and concentration polarization regions. For instance, when the current density is at 1.1 A/cm^2, a drop of nearly 5% in the cell voltage can be seen after 30,000 cycles. Clearly, the majority of the reduction in performance occurs in the concentration polarization regime. When the current density is at 2.1 A/cm^2, a drop of the cell voltage from 0.45 A/cm^2 to 0.39 A/cm^2 can be observed, and the maximum power density is 0.84 W/cm^2 after 30,000 AST cycles. The Nyquist plots for the MEA prepared by HSC-Pt5 before and after the accelerated stress tests are presented in Fig. 8(c). It is clear that the single impedance arc after 30,000 cycles shows higher resistance in ohmic and charge transfer area which can be related to the catalyst layer degradation and restructuring [48]. These results are well consistent with the drop in cyclic voltammograms and polarization curves.

Fig. 9 presents the polarization and power density curves of the MEA prepared by HSC-Pt5 before and after 30,000 cycling of AST under the low RH condition of 40%, at a cell temperature of 75 °C and backpressure of 35 kPag. As shown in the graph, the cell performances before and after the ASTs in the activation polarization regime are almost the same, and a slight decrease starts at the ohmic polarization regime, e.g., when the current density is at 0.5 A/ cm^2, the cell voltage declines by 6%. This reduction is increased in the concentration polarization regime, as the cell voltage is dropped by 37% at the current densities of 1.7 A/ cm^2. These results also demonstrate the prominent impact of the morphological and microstructural changes in the catalyst layer in single cell test which are more evident at the low RH and low flow of reactants [48]. The maximum power density is also dropped by 20% which is 7% more than the drop at the fully humidified condition. In spite of higher cell performance drop under the low RH condition, it should be noted that the maximum power density of 0.5 W/cm^2 after 30,000 cycles of AST under the low flow of reactants and partial humidification of 40% RH can be considered as excellent, and highly acceptable when compared with the cell performances reported under similar conditions in literature.

4. Conclusions

In this study, one-pot synthesis method is employed for preparing the size-controlled platinum (Pt) nanoparticles on functionalized high surface area carbon (HSC). Pt nanoparticles with two different sizes of 2 nm and 5 nm are prepared by controlling the reaction temperature at 180 °C and 160 °C, respectively. Based on the physical characterizations, both catalysts have non-spherical shape which are well dispersed on HSC surface without any agglomeration. In addition, they have face centered cubic (fcc) crystallinity phases and total loading of around 45% on HSC. The in-situ and ex-situ electrochemical characterization results indicate that fuel cell performance and electrochemical surface area are strongly influenced by the size of the Pt nanoparticles. Half-cell results elucidate the prominent role of Pt nanoparticle sizes on the active surface area, mass activity and durability, while the full-cell data shows the impact of Pt nanoparticle sizes on the catalyst layer morphology and structure, and it is found that the electrochemical surface area and maximum power densities of the full cell made of the 2 nm Pt nanoparticles are higher than the MEA made of the 5 nm Pt nanoparticles under

the different relative humidity (RH) and flow rates of reactants. Ex-situ accelerated stress tests (AST) show that HSC with 5 nm particles have better durability compared to that with 2 nm. In-situ AST results for the MEA prepared with the 5 nm Pt nanoparticles shows 13% reduction in the maximum power density after 30,000 cycles, with the maximum power density of 0.84 W/cm^2 under the fully humidified condition; and 20% decrease with the maximum power density of 0.5 W/cm^2 after 30,000 cycles of AST under the partial humidification of 40%, illustrating the excellent performance and durability of the catalyst and the fuel cell developed in this study.

Declaration of Competing Interest

The authors declare that they have no known competing financial interests or personal relationships that could have appeared to influence the work reported in this paper.

Acknowledgement

This work received financial support from Canadian Urban Transit Research and Innovation Consortium (CUTRIC) via Project Number 160028, Natural Sciences and Engineering Research Council of Canada (NSERC) via a Discovery Grant.

References

[1] Li X. Principles of fuel cells. CRC Press; 2005.
[2] Larminie J, Dicks A, McDonald MS. Fuel cell systems explained, 2. Chichester, UK: J. Wiley; 2003.
[3] He H, Quan S, Sun F, Wang YX. Model predictive control with lifetime constraints based energy management strategy for proton exchange membrane fuel cell hybrid power systems. IEEE Trans Indust Electron 2020;67(10):9012–23.
[4] Gasteiger HA, Kocha SS, Sompalli B, Wagner FT. Activity benchmarks and requirements for Pt, Pt-alloy, and non-Pt oxygen reduction catalysts for PEMFCs. Appl Catal B 2005.
[5] Prokop M, Drakselova M, Bouzek K. Review of the experimental study and prediction of Pt-based catalyst degradation during PEM fuel cell operation. Curr Opin Electrochem 2020;20:20–7.
[6] Wang Y, Diaz DFR, Chen KS, Wang Z, Adroher XC. Materials, technological status, and fundamentals of PEM fuel cells–a review. Mater Today 2020;32:178–203.
[7] Shahgaldi S, Ozden A, Li X, Hamdullahpur F. A novel membrane electrode assembly design for proton exchange membrane fuel cells: characterization and performance evaluation. Electrochim Acta 2019;299:809–19.
[8] Shahgaldi S, Alaefour I, Li X. Impact of manufacturing processes on proton exchange membrane fuel cell performance. Appl Energy 2018;225:1022–32.
[9] Shahgaldi S, Ozden A, Li X, Hamdullahpur F. Cathode catalyst layer design with gradients of ionomer distribution for proton exchange membrane fuel cells. Energy Convers Manage 2018;171:1476–86.
[10] Kinoshita K. Particle size effects for oxygen reduction on highly dispersed platinum in acid electrolytes. J Electrochem Soc 2017;137(3).
[11] Nesselberger M, Ashton S, Meier JC, Katsounaros I, Mayrhofer KJJ, Arenz M. The particle size effect on the oxygen reduction reaction activity of Pt catalysts: influence of electrolyte and relation to single crystal models. J. Am. Chem. Soc. 2011;133(43):17428–33.
[12] Wang C, Daimon H, Onodera T, Koda T, Sun S. A general approach to the size-and shape-controlled synthesis of platinum nanoparticles and their catalytic reduction of oxygen. Angew Chem Int Ed 2008;47(19):3588–91.
[13] Maciá MD, Campiña JM, Herrero E, Feliu JM. On the kinetics of oxygen reduction on platinum stepped surfaces in acidic media. J Electroanal Chem 2004;564(1–2):141–50.
[14] Campbell CT, Parker SC, Starr DE. The effect of size-dependent nanoparticle energetics on catalyst sintering. Science 2002;298(5594):811–14.
[15] Wilson MS, Garzon FH, Sickafus KE, Gottesfeld S. Surface area loss of supported platinum in polymer electrolyte fuel cells. J Electrochem Soc 1993;140(10):2872.
[16] Bett JAS, Kinoshita K, Stonehart P. Crystallite growth of platinum dispersed on graphitized carbon black: II. Effect of liquid environment. J Catal 1976;41(1):124–33.
[17] Wikander K, Ekström H, Palmqvist AEC, Lindbergh G. On the influence of Pt particle size on the PEMFC cathode performance. Electrochim. Acta 2007;52(24):6848–55.
[18] Shao Y, Yin G, Gao Y. Understanding and approaches for the durability issues of Pt-based catalysts for PEM fuel cell. J Power Sources 2007;171(2):558–66.
[19] Holby EF, Sheng W, Shao-Horn Y, Morgan D. Pt nanoparticle stability in PEM fuel cells: influence of particle size distribution and crossover hydrogen. Energy Environ Sci 2009;2(8):865–71.
[20] Borup RL, Davey JR, Garzon FH, Wood DL, Inbody MA. PEM fuel cell electrocatalyst durability measurements. J Power Sources 2006;163(1):76–81 SPEC. ISS..
[21] Xu Z, Zhang H, Zhong H, Lu Q, Wang Y, Su D. Effect of particle size on the activity and durability of the Pt/C electrocatalyst for proton exchange membrane fuel cells. Appl Catal, B 2012;111–112:264–70.
[22] Yano H, Watanabe M, Iiyama A, Uchida H. Particle-size effect of Pt cathode catalysts on durability in fuel cells. Nano Energy 2016;29:323–33.
[23] Shahgaldi S, Hamelin J. Improved carbon nanostructures as a novel catalyst support in the cathode side of PEMFC: a critical review. Carbon N Y 2015;94:705–28.
[24] Antolini E. Carbon supports for low-temperature fuel cell catalysts. Appl Catal B 2009;88(1–2):1–24.
[25] Shahgaldi S, Hamelin J. Stability study of ultra-low Pt thin film on TiO_2–C core–shell structure and TiO_2 encapsulated in carbon nanospheres as cathode catalyst in PEMFC. Fuel 2015;150:645–55.
[26] Auer E, Freund A, Pietsch J, Tacke T. Carbons as supports for industrial precious metal catalysts. Appl Catal A 1998;173(2):259–71.
[27] Guha A, Lu W, Zawodzinski TA, Schiraldi DA. Surface-modified carbons as platinum catalyst support for PEM fuel cells. Carbon N Y 2007;45(7):1506–17.
[28] Ghasemi M, Shahgaldi S, Ismail M, Kim BH, Yaakob Z, Daud WRW. Activated carbon nanofibers as an alternative cathode catalyst to platinum in a two-chamber microbial fuel cell. Int J Hydrogen Energy 2011;36(21):13746–52.
[29] Veizaga N, Fernandez J, Bruno M, Scelza O, De Miguel S. Deposition of Pt nanoparticles on different carbonaceous materials by using different preparation methods for PEMFC electrocatalysts. Int J Hydrogen Energy 2012;37(23):17910–20.
[30] Moghaddam RB, Shahgaldi S, Li X. A facile synthesis of high activity cube-like Pt/carbon composites for fuel cell application. Front Energy 2017;11(3):245–53.
[31] Shahgaldi S, Hamelin J. The effect of low platinum loading on the efficiency of PEMFC's electrocatalysts supported on TiO_2–Nb, and SnO_2–Nb: an experimental comparison between active and stable conditions. Energy Convers Manage 2015;103:681–90.
[32] Zhang J. PEM fuel cell electrocatalysts and catalyst layers: fundamentals and applications. Springer Science & Business Media; 2008.
[33] Pollet BG. A novel method for preparing PEMFC electrodes by the ultrasonic and sonoelectrochemical techniques. Electrochem Commun 2009;11(7):1445–8.
[34] Vinayan BP, Jafri RI, Nagar R, Rajalakshmi N, Sethupathi K, Ramaprabhu S. Catalytic activity of platinum–cobalt alloy nanoparticles decorated functionalized multiwalled carbon nanotubes for oxygen reduction reaction in PEMFC. Int J Hydrogen Energy 2012;37(1):412–21.
[35] Yaldagard M, Jahanshahi M, Seghatoleslami N. Carbonaceous nanostructured support materials for low temperature fuel cell electrocatalysts—a review. World J Nano Sci Eng 2013 2013.
[36] Sriring N, Tantavichet N, Pruksathorn K. Preparation of Pt/C catalysts by electroless deposition for proton exchange membrane fuel cells. Korean J Chem Eng 2010;27(2):439–45.
[37] Shinozaki K, Zack JW, Richards RM, Pivovar BS, Kocha SS. Oxygen reduction reaction measurements on platinum electrocatalysts utilizing rotating disk electrode technique I. Impact of impurities, measurement protocols and applied corrections. J Electrochem Soc 2015;162(10):F1144–58.
[38] Gilman S. A study of the mechanism of carbon monoxide adsorption on platinum by a new electrochemical procedure 1. J Phys Chem 1963;67(1):78–84.
[39] Leonard N, Nallathambi V, Barton SC. Carbon supports for non-precious metal oxygen reducing catalysts. J Electrochem Soc 2013;160(2013):F788–92.
[40] Zhao J, Ozden A, Shahgaldi S, Alaefour IE, Li X, Hamdullahpur F. Effect of Pt loading and catalyst type on the pore structure of porous electrodes in polymer electrolyte membrane (PEM) fuel cells. Energy 2018;150:69–76.
[41] Wang S, Chen S, Ma L, Zapien JA. Recent progress in cobalt-based carbon materials as oxygen electrocatalysts for zinc-air batteries applications. Mater Today Energy 2021:100659.
[42] Shahgaldi S, Hamelin J. Improved carbon nanostructures as a novel catalyst support in the cathode side of PEMFC: a critical review. Carbon N Y 2015;94:705–28.
[43] Xu Z, Zhang H, Zhong H, Lu Q, Wang Y, Su D. Effect of particle size on the activity and durability of the Pt/C electrocatalyst for proton exchange membrane fuel cells. Appl Catal, B 2012;111:264–70.
[44] Kumpulainen H, Peltonen T, Koponen U, Bergelin M, Valkiainen M, Wasberg M. In situ voltammetric characterization of PEM fuel cell catalyst layers, 2137. Technical Research Centre of Finland; 2002. p. 28. Research Notes.
[45] Mohsin M, Raza R, Mohsin-ul-Mulk M, Yousaf A, Hacker V. Electrochemical characterization of polymer electrolyte membrane fuel cells and polarization curve analysis. Int J Hydrogen Energy 2019.
[46] Hsieh S, Su Y. Effects of anode and cathode perforated flow field plates on proton exchange membrane fuel cell performance. Int J Energy Res 2014;38(7):944–53.
[47] Jung J-H, Cha M-S, Kim J-B. Optimization of nafion ionomer content using synthesized Pt/carbon nanofibers catalyst in polymer electrolyte membrane fuel cell. J Nanosci Nanotechnol 2012;12(7):5412–17.
[48] Shahgaldi S, Ozden A, Li X, Hamdullahpur F. A scaled-up proton exchange membrane fuel cell with enhanced performance and durability. Appl Energy 2020;268:114956.